C O N V E C T I O N D E V E L O P M E N T

I N A S H E A R E D W I N D F I E L D

TECHNICAL REPORT

MARJAN DIVJAK

HYDROMETEOROLOGICAL INSTITUTE OF SLOVENIA

LJUBLJANA, YUGOSLAVIA

JULY 1988

TABLE OF CONTENTS

LIST OF SYMBOLS

c_H	Evaporation parameterization constant	1×10^{-4} /s
c_P	Specific heat of air at constant pressure	1.0×10^{3} J/kgK
c_R	Evaporation parameterization constant	1×10^{-3} /s
e_o	Saturation water vapour pressure at 0°C	6.1×10^{2} N/m^2
g	Acceleration of gravity	9.8 m/s^2
K	Turbulence parameterization constant	500 m^2/s
k_A	Accretion parameterization constant	2/s
k_C	Conversion parameterization constant	1×10^{-3} /s
k_H	Fallspeed parameterization constant	24 m/s
k_R	Fallspeed parameterization constant	14 m/s
L_V	Latent heat of condensation	2.5×10^{6} J/kg
p	Pressure	
P_C	Cloud hydrometeors production term	
P_P	Precipitating hydrometeors production term	
P_V	Water vapour production term	
q_c	Cloud hydrometeors mixing ratio	
q_P	Precipitating hydrometeors mixing ratio	
q_s	Saturated water vapour mixing ratio	
q_V	Water vapour mixing ratio	
q_o	Conversion parameterization constant	1×10^{-3}
R_V	Gas constant of water vapour	461 J/kgK
t	Time	
T	Temperature	
T_o	Microphysical parameterization constant	0°C
T_A	Microphysical parameterization constant	20°C
T_B	Microphysical parameterization constant	-20°C
T_C	Microphysical parameterization constant	-40°C
u	Air velocity in the x-direction	
v	Air velocity in the y-direction	
$\bar{v}_H$	Mass-weighted mean fallspeed of hailstones	
$\bar{v}_P$	Mass-weighted mean fallspeed of the precipitating hydrometeors	
$\bar{v}_R$	Mass-weighted mean fallspeed of rain drops	
$\mathcal{V}$	Air velocity	
w	Vertical air velocity	
x	Horizontal coordinate	
y	Horizontal coordinate	
z	Vertical coordinate	
ε	Shorthand constant	0.62
Θ	Potential temperature	
Θ^*	Normalized potential temperature $\Theta^*=(\Theta-\bar{\Theta})/\bar{\Theta}$, $\bar{\Theta}=\Theta(p=p_o)$	
π	Non-dimensional pressure $\pi=(p/p_o)^{R_d/c_P}$, p_o=1000 mb, R_d/c_P=0.286	
ϱ	Air density	

1. INTRODUCTION

The life cycle of an isolated convective storm is dependent on a large number of atmospheric conditions; among these are the ambient temperature and humidity fields, the ambient wind profile, the nature of the cloud microphysical processes, surface heating and topography. One of the aims of theoretical studies of convective storms is to investigate the effects of variations of these parameters.

In this report, the effects of the ambient wind profile on the convection development are studied. From the great variety of possible ambient wind patterns, three typical and qualitatively different profiles are used for investigations: no ambient wind, unidirectional positive wind shear, and multidirectional wind shear dominated by strong low level veering. Temperature and humidity fields used, and microphysical processes included are directed specifically toward the studying of mid-latitude summertime continental thunderstorms.

2. NUMERICAL MODEL

2.1 Assumptions

The system modeled is the atmosphere (air with hydrometeors) in a limited domain over the earth surface. The domain is a rectangular prism with open lateral boundaries and rigid upper and bottom boundaries. It is translated steadily relative to the earth with the appropriate velocity to keep convective disturbances well inside.

Air motions are anelastic (without acoustic waves) and influenced by the following forces: gravity, pressure gradient force, hydrometeor drag, and internal (eddy) friction. The external friction at the earth surface and the Coriolis force are neglected.

Hydrometeors are partitioned into two classes - cloud hydrometeors (water droplets and ice crystals with a negligible fallspeed), and precipitating hydrometeors (raindrops, graupel, hail). All hydrometeors have the same horizontal velocity component as the air; cloud hydrometeors have zero terminal fallspeed relative to air; precipitating hydrometeors fall with a "representative" fallspeed.

Any supersaturation is locally removed through instantaneous condensation / deposition into cloud hydrometeors and release of latent heat. Latent heat of

freezing is neglected. Cloud hydrometeors in unsaturated air instantaneously evaporate / sublime until saturation is reached or all hydrometeors are consumed. In the absence of cloud hydrometeors, precipitating hydrometeors evaporate / sublime with a given rate. Latent heat of melting is neglected. Moistening of the boundary layer from the ground is not included.

Precipitating hydrometeors are generated from cloud hydrometeors in the "precipitation formation layer" between -20 and -40°C with a given rate, simulating cloud droplets freezing and subsequent growth by vapour deposition and riming. Precipitating hydrometeors grow with a given rate by the gravitational sweep-out of the cloud hydrometeors.

2.2 Equations

2.2.1 Main equations

Mathematical framework of the model consists of the following eight equations for the eight model fields. All symbols used are explained in the List of Symbols. The quantities with overbars represent the hydrostatically balanced initial environment, whereas the quantities with prime subscripts represent its perturbations. The underlined quantities are functions of model variables, the dependence being given by closing equations. Since all the equations are well known, no derivation of them is given in this report.

Dynamics:

$$\partial w/\partial t = - (w\nabla)w + K\nabla^2 w' - g(\theta^{*\prime}+\varepsilon q_v'-q_c-q_p) - c_p\bar{\theta}\nabla\pi'.$$

The terms on the right represent, from left to right, the changes in velocity due to advection, turbulent diffusion, buoyant acceleration, hydrometeor drag, and pressure perturbation.

Pressure diagnostics:

$$c_p\nabla\bar{\rho}\bar{\theta}\nabla\pi' = - \nabla[\bar{\rho}(w\nabla)w] + K\nabla[\bar{\rho}\nabla^2 w'] - g\partial[\bar{\rho}(\theta^{*\prime}+\varepsilon q_v'-q_c-q_p)]/\partial z.$$

Thermodynamics:

$$\partial\theta^*/\partial t = - w\nabla\theta^* + K\nabla^2\theta^{*\prime} + (L_v/c_p\bar{\pi}\bar{\theta})P_v.$$

The terms on the right represent contributions due to advection, turbulent diffusion, and condensation / evaporation.

Continuity of water substance:

$$\partial q_v/\partial t = - w\nabla q_v + K\nabla^2 q'_v + P_v \quad ,$$

$$\partial q_c/\partial t = - w\nabla q_c + K\nabla^2 q_c + P_c \quad ,$$

$$\partial q_p/\partial t = - w\nabla q_p + \bar{v}_p \partial q_p/\partial z + P_p \, .$$

The terms on the right represent contributions due to advection, turbulent diffusion (non-precipitating water only), sedimentation (precipitating water only), and microphysical processes.

2.2.2 Closing equations

Main equations of the model are closed with the following equations for the hydrometeor fallspeeds and water substance production terms. All the constants used are listed in the List of Symbols.

Hydrometeor fallspeeds are given by

$$\bar{v}_p = \begin{cases} \bar{v}_R & , \; T > T_A \quad , \\ \bar{v}_H & , \; T < T_o \quad , \\ [(T-T_o)\bar{v}_R + (T_A-T)\bar{v}_H]/(T_A-T_o) & , \; \text{otherwise} \quad , \end{cases}$$

with

$$\bar{v}_R = k_R q_p^{1/8} \quad ,$$

$$\bar{v}_H = k_H q_p^{1/8} \quad .$$

Water substance production terms are decomposed into the following partial production terms:

$$P_v = (P_{cve} - P_{vck}) + P_{pve} \quad ,$$

$$P_c = - (P_{cve} - P_{vck}) - P_{cpc} - P_{cpa} \quad ,$$

$$P_p = - P_{pve} + P_{cpc} + P_{cpa} \quad .$$

Production term P_{ABC} is the rate of change of the mixing ratio "A", transforming into "B" in the manner "C" (V - vapour, C - cloud hydrometeors, P - precipitating hydrometeors; C - conversion, A - accretion, E - evaporation, K - condensation).

The quantity $(P_{cve} - P_{vck})\Delta t$ is given by the amount needed for instantaneous saturation adjustment till $q_s = (\varepsilon e_o/\bar{p})\exp[(L_v/R_v)(1/T_o - 1/T)]$. Other partial production terms are approximated in the following way:

$$P_{PVE} = \begin{cases} c_R(q_s - q_v) & , T \geq T_o \text{ and } q_s > q_v, \\ c_H(q_s - q_v) & , T < T_o \text{ and } q_s > q_v; \end{cases}$$

$$P_{CPC} = \begin{cases} k_c(q_c - q_o) & , q_c > q_o \text{ and } T_C < T < T_B, \\ 0 & , \text{otherwise.} \end{cases}$$

$$P_{CPA} = \begin{cases} k_A q_c q_p^{7/8} & , q_c > q_o \text{ and } T > T_c. \\ 0 & , \text{otherwise.} \end{cases}$$

2.3 Boundary conditions

2.3.1 Lower boundary

The lower surface is assumed rigid and free slip:

$$w = \partial u/\partial z = \partial v/\partial z = 0.$$

For condensed water, zero normal gradients are assumed, i.e.,

$$\partial q_c/\partial z = \partial q_p/\partial z = 0,$$

and for temperature and humidity the following boundary conditions are used:

$$\theta^{*\prime} = 0, \; w > 0 \; ,$$

$$\partial\theta^{*\prime}/\partial z = 0, \text{ otherwise;}$$

$$q_v' = 0 \; , \; q_v < q_s \; ,$$

$$q_v = q_s, \text{ otherwise.}$$

The boundary condition on pressure is consistent with the third equation of motion:

$$\partial\pi'/\partial z = (g/c_p\bar{\theta})(\theta^{*\prime} + \varepsilon q_v' - q_c - q_p).$$

2.3.2 Upper boundary

Like the lower boundary, the upper boundary is assumed rigid and free slip. Moisture, condensed water, and temperature are maintained undisturbed:

$$q' = q_c = q_p = \theta^{*\prime} = 0.$$

The upper boundary condition on pressure is the same as for the lower boundary.

2.3.3 Lateral boundaries

For temperature, moisture, condensed water, and tangential velocity components across lateral boundaries, zero horizontal gradients are assumed. At x=0, for instance,

$$\partial v/\partial x = \partial w/\partial x = \partial \theta^{*\prime}/\partial x = \partial q_v'/\partial x = \partial q_c/\partial x = \partial q_r/\partial x = 0.$$

The normal acceleration at the boundary is assumed zero initially, and for all later time steps it is set equal to $0.8\ \partial u/\partial t$ at a distance Δx inward from the boundary for the preceeding time step. The boundary condition on pressure is consistent with the first equation of motion:

$$\partial \pi'/\partial x = (1/c_p\bar{\theta})[-\ w\nabla u + K\nabla^2 u' - (\partial u/\partial t)].$$

Analogous conditions are used at other lateral boundaries.

2.4 Numerical implementation

Model equations are solved by the finite difference method. The domain is divided into 50x50x26 equal volume elements. The size of the volume element is 1x1x0.5 km, and the size of the domain is 50x50x13 km. At the mid-points of the faces of the volume element, velocity components normal to the faces are computed; all other variables are computed at the center of the volume element.

For the velocity and temperature advection, the forward in time / upstream in space scheme is used. The correction term for counteracting the pseudo-diffusive effect inherent in this scheme is not included. To prohibit the unstable gravity wave growth, the thermal vertical advection term at the time level n is evaluated using the vertical velocity from time level n+1. For the advection of mixing ratios, the forward in time / flux-upstream in space scheme is used. No corrections for counteracting the pseudo-diffusive effect of the scheme are made. For the diffusion, the forward in time / centered in space scheme is used. All other spacial derivatives are approximated by centered differences.

Time step is fixed: 10 sec.

Pressure diagnostic equation is solved by the overrelaxation method. To keep the divergence $D=\nabla\bar{\rho}v$

from building up with time, the term $\partial D/\partial t$ is retained in the pressure diagnostic equation and approximated as $-D^{(n)}/\Delta t$. Sweep directions are changed at each time level. Pressure field is normalized by requiring the grand mean of pressure perturbations over the lateral boundaries to be zero.

3. INITIAL CONDITIONS

3.1 Base states

To investigate the effects of the ambient wind profile on the convection development, three numerical experiments are carried out. For each of these experiments, the same initial temperature and humidity fields and a qualitatively different initial wind field are used: no wind shear (C-case), positive speed shear but no directional shear (S-case), and positive speed shear with low level veering (V-case). The initial temperature and humidity profiles are shown on Fig. 1, and the three initial wind profiles are presented on Figs. 2, 3, and 4. Temperature, humidity, and wind profiles used are typical for mid-latitude summertime continental thunderstorm environments.

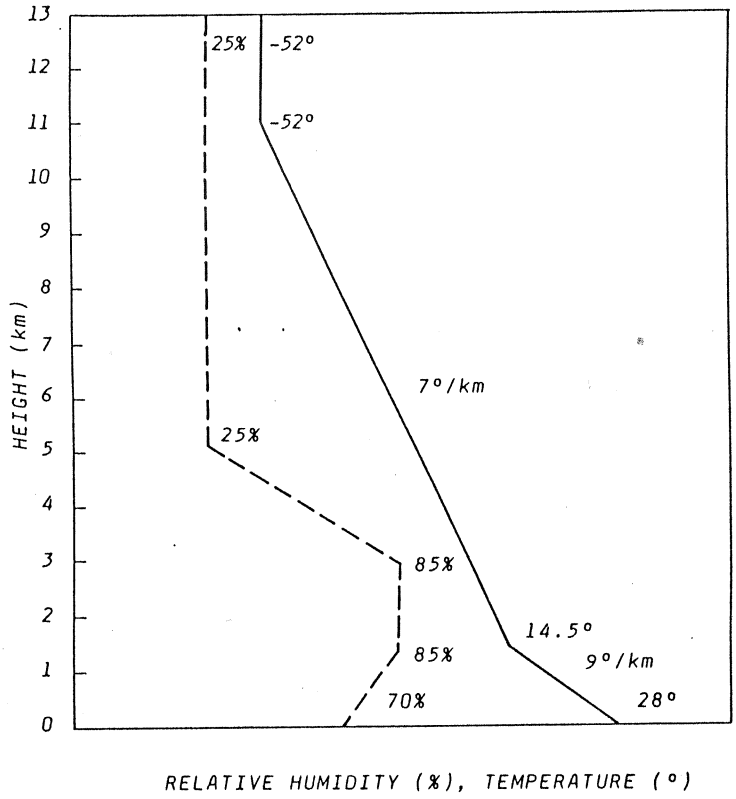

Fig. 1: Initial temperature (full line) and humidity (dashed line) profiles.

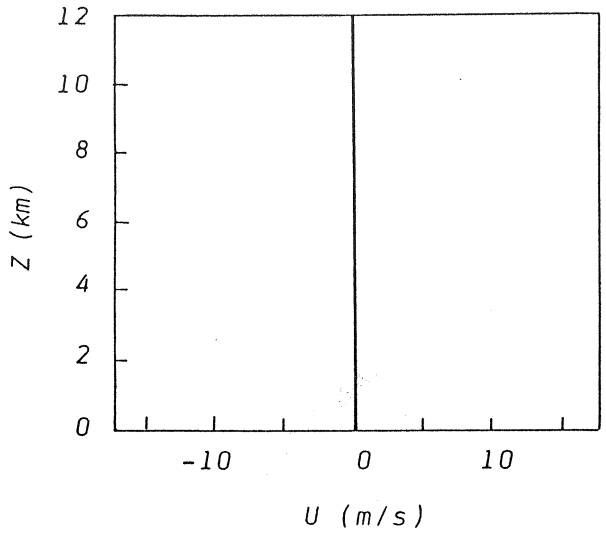

Fig. 2: Initial wind profile for the C-case.

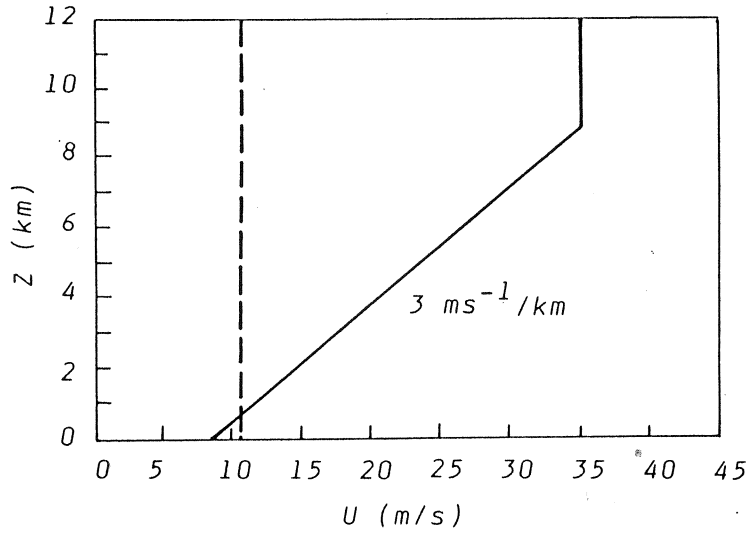

Fig. 3: Initial wind profile for the S-case. The dashed line represents the domain velocity.

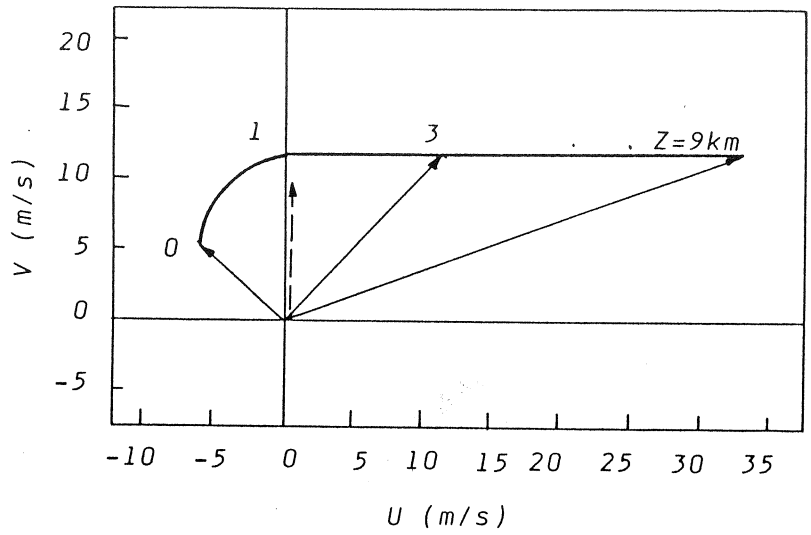

Fig. 4: Initial wind profile for the V-case. The dashed vector represents the domain velocity.

3.2 Initial perturbations

For the three numerical experiments three different initial perturbations are used. All of them take the form of a shallow radial symmetric warm updraft located in the domain interior. The perturbations are described on Fig. 5. They produce convective disturbances of nearly the same intensity in all three cases.

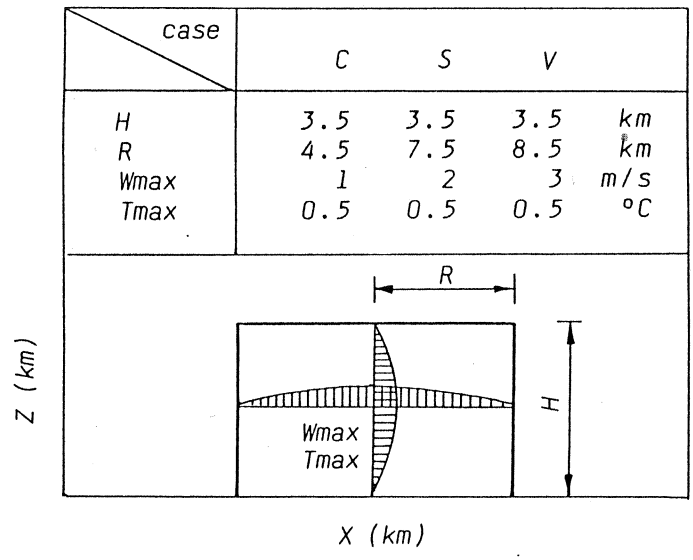

Fig. 5: Initial perturbations used in the C, S, and V-case.

4. RESULTS OF NUMERICAL EXPERIMENTS

The output from numerical experiments for each case consists of three-dimensional fields of all variables at 5 minute intervals. Only a selection of this material is presented here. The life cycle of the convective storm in each case is presented in three typical time points, when the storm reaches the growing, mature, and dissipating stage. In these time points, fields are displayed in appropriate cross - sections. Only a part of the computational domain is shown. The scale origin of the horizontal axes is set to the center of the initial perturbation. Vertical cross - sections begin at the lower domain boundary. Horizontal ticks are plotted at 1 km intervals and vertical ticks at 0.5 km intervals. Cloud hydrometeor concentrations are plotted with solid lines, and precipitating hydrometeor concentrations with dashed lines with thick lines denoting 0.01 g/kg values. Wind vectors are plotted relative to the (moving) domain. For all other fields, positive contours are solid, negative contours are dashed, and zero contours are not included.

The panel headings have the following structure: field variable (unit, contour interval or vector scale factor), plane type (plane location), time, case indicator. Field variables have the following names: UW - wind vector component in the xz-plane, W - vertical air velocity, DPH - non-dimensional pressure perturbation, DTH - potential temperature perturbation, QW and QI - nonprecipitating and precipitating hydrometeors mixing ratios, DIV - horizontal divergence, VOR - vertical component of vorticity. Due to programming error, divergence and vorticity units (s^{-1}) are not indicated in the panel headings. In some cases, two contour intervals are given; the first one is for positive field values, the second one for negative ones. Vector scale factors denote the absolute value of the wind vector of the inter-tick length. The first factor stands for the horizontal vector component and the horizontal inter-tick length, and the second one for the vertical vector component and the vertical inter-tick length. Plane types are denoted by XZ, YZ, or XY, according to the field cross-section type. The location of the cross-section plane is given relative to the bottom boundary center of the initial perturbation. Time is given in minutes and case is indicated by C1, S1, and V1 symbols. In addition to detailed field cross-sections, a general cloud life history is presented for each case cloud, i.e., maximum and minimum vertical velocities, and maximum precipitating water

mixing ratio for the entire domain interior, and maximum precipitation rate at the lower boundary are shown as functions of time. Time points of the growing, mature, and dissipating stage displays are marked with black arrows. Numbers over specific maxima indicate their heights (in km) in the domain.

4.1 No shear case (C-case)

4.1.1 Growing stage (Figs. 6a-6f)

From the initial perturbation, the updraft develops and compensating downdrafts form in its surrounding at middle levels. The perturbed pressure field exhibits a meso-low under the cloud, and a meso high near its top. Temperature perturbations are positive in the cloud and negative above its top and at its base. Thermal buoyancy and the perturbed vertical pressure gradient force oppose each other. First precipitating hydrometeors are formed at the cloud top, when its temperature reaches -20 C. They are carried upwards, forming an accumulation zone above the updraft maximum.

4.1.2 Mature stage (Figs. 7a-7f)

As the cloud top approaches the tropopause, upper level gravity wave is generated. Precipitating hydrometeors begin to fall through the outer updraft regions and reach the ground, partially reentering the updraft at low levels. Low level downdraft develops under the updraft and upper level updraft weakens. The perturbed pressure field shows a meso-high beneath the downdraft.

4.1.3 Dissipating stage (Figs. 8a-8f)

Vertical velocities weaken. Precipitations gradualy cease. All fields approach the initial nonperturbed state.

4.1.4 General life history (Fig. 9)

The updraft develops rapidly until the first precipitations are formed but the precipitation loading and the tropopause gradually stop its growth. The oscillation of the updraft and precipitation maxima is partially caused by the interaction between the updraft, tropopause, and precipitation loading and partially by the initial perturbation. After reaching its maximum value, the updraft weakens rapidly and the low-level downdraft develops. Updraft and downdraft maxima are well displaced in time.

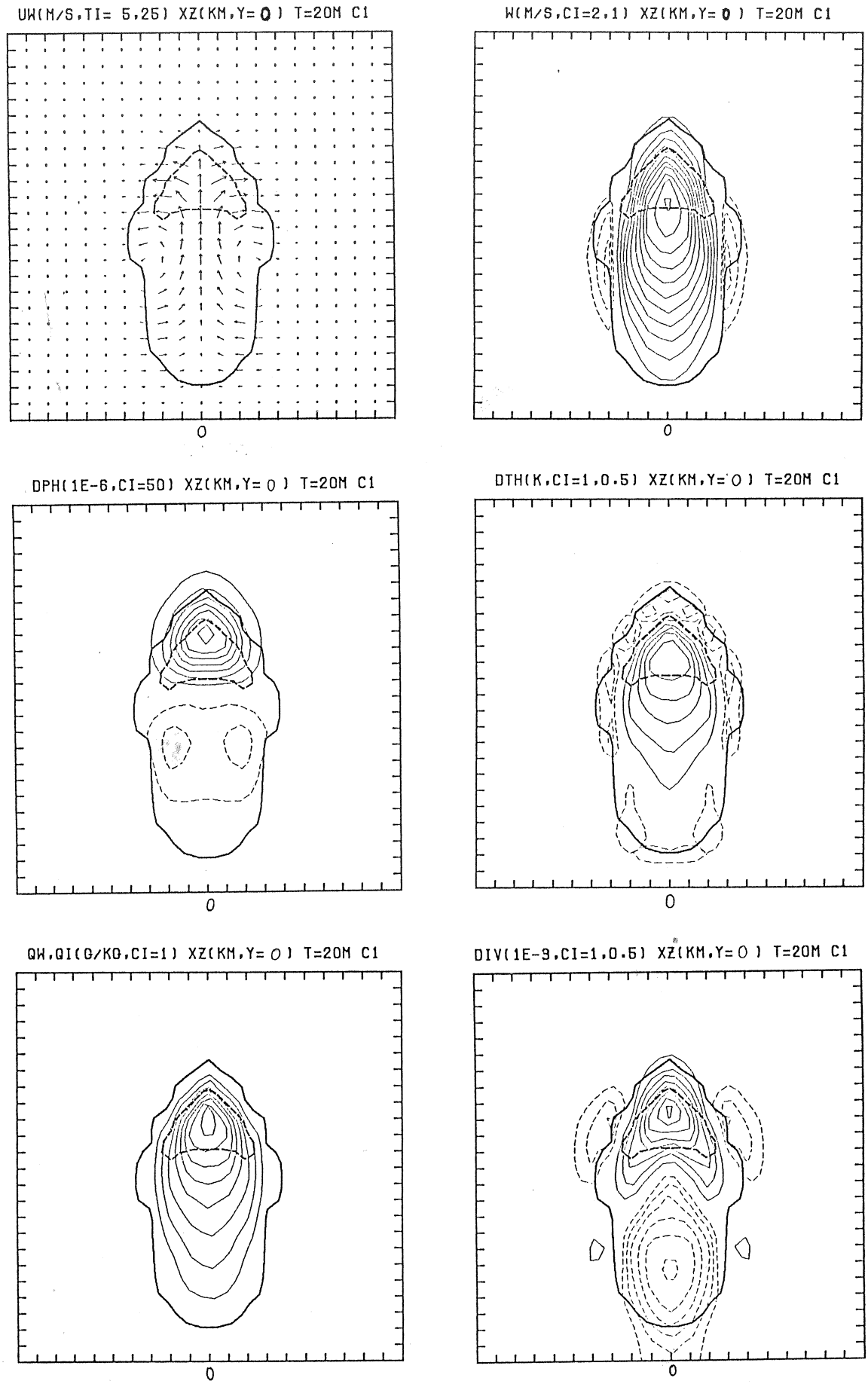

Figs. 6a - 6f: C-case, growing stage.

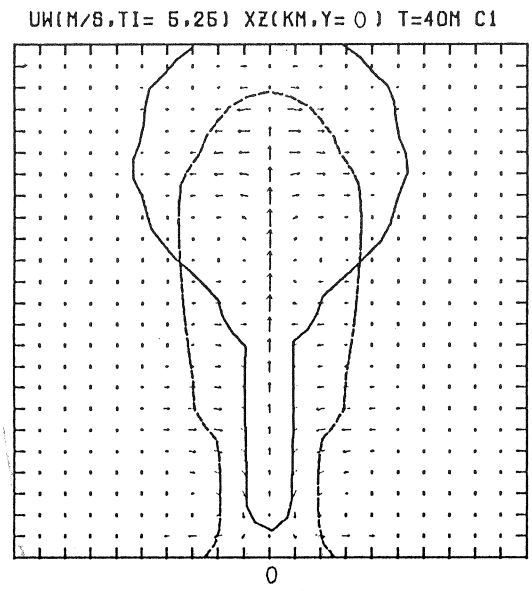

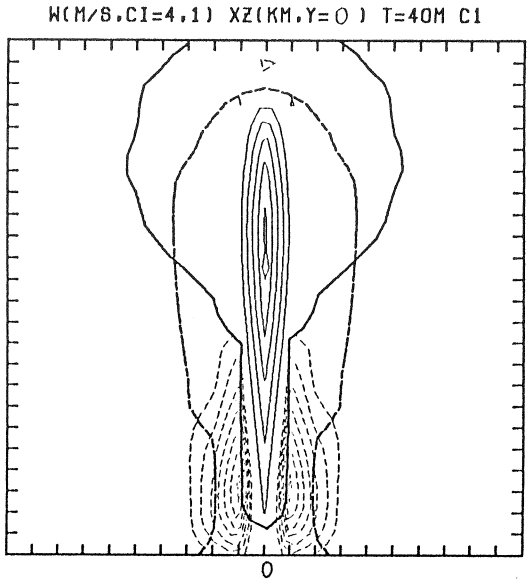

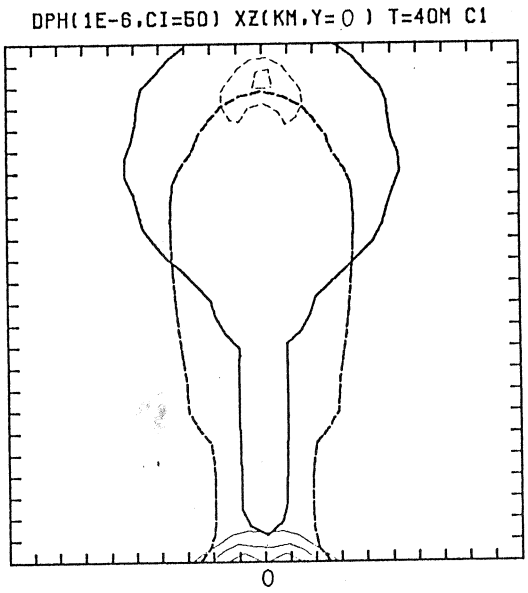

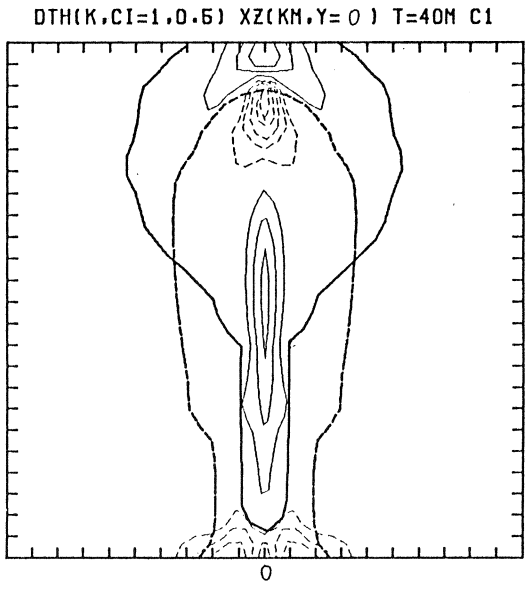

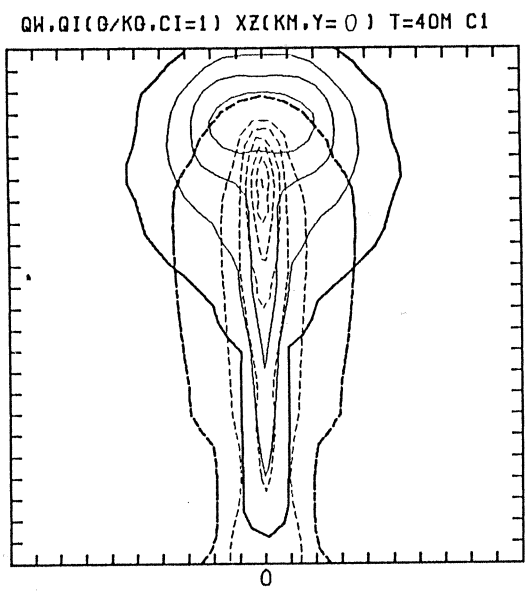

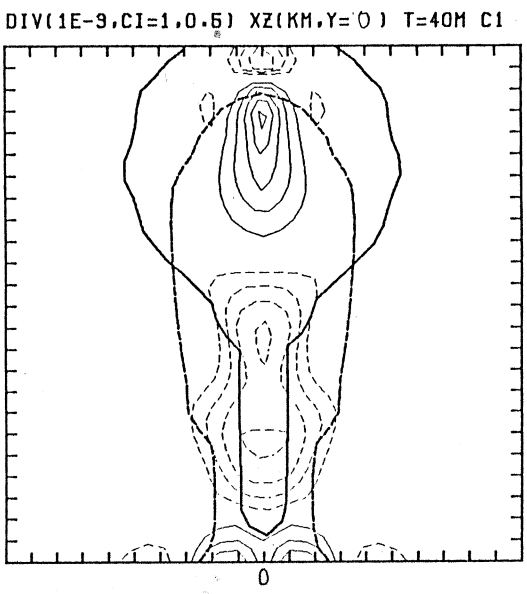

Figs. 7a - 7f: C-case, mature stage.

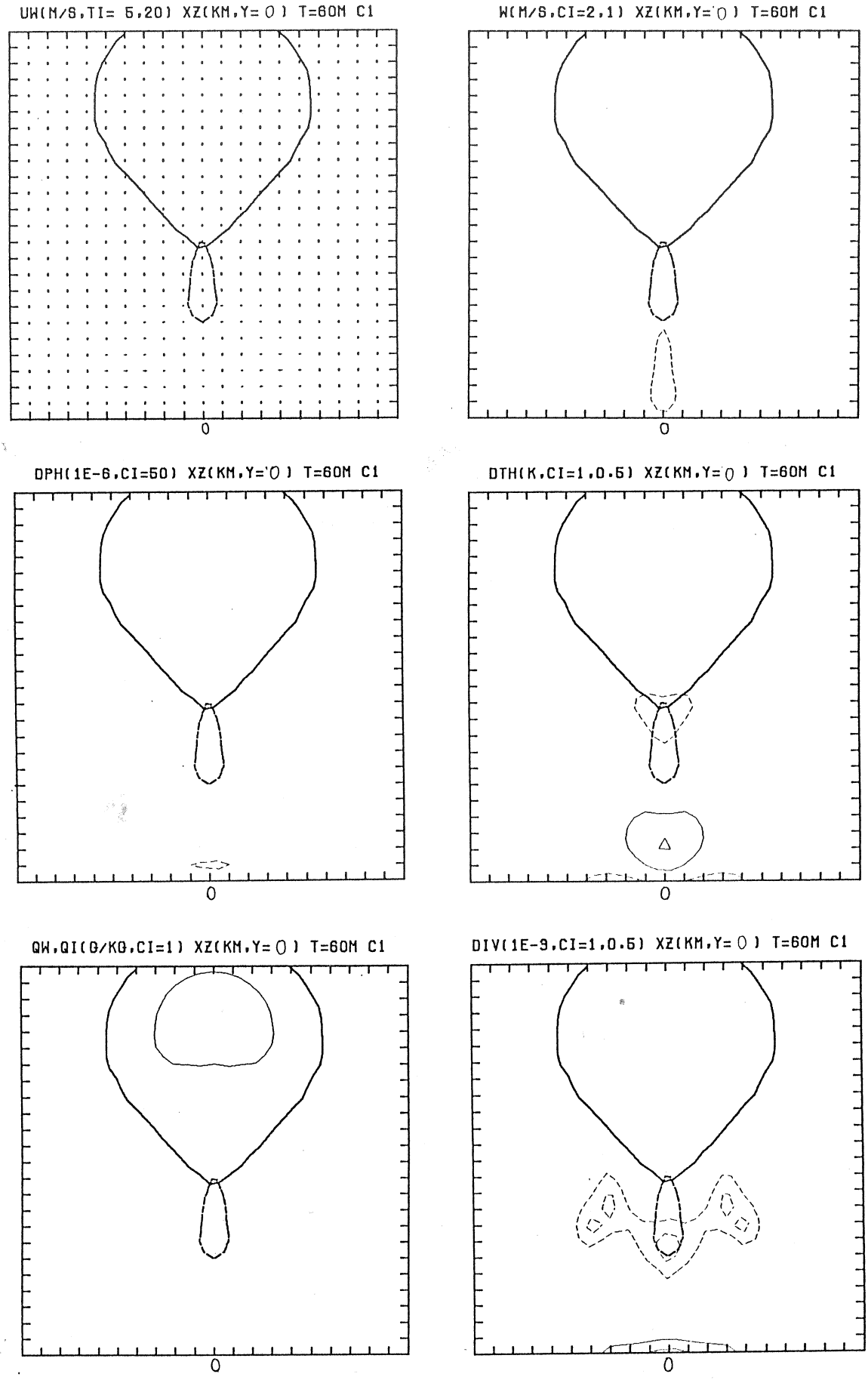

Figs. 8a - 8f: C-case, dissipating stage.

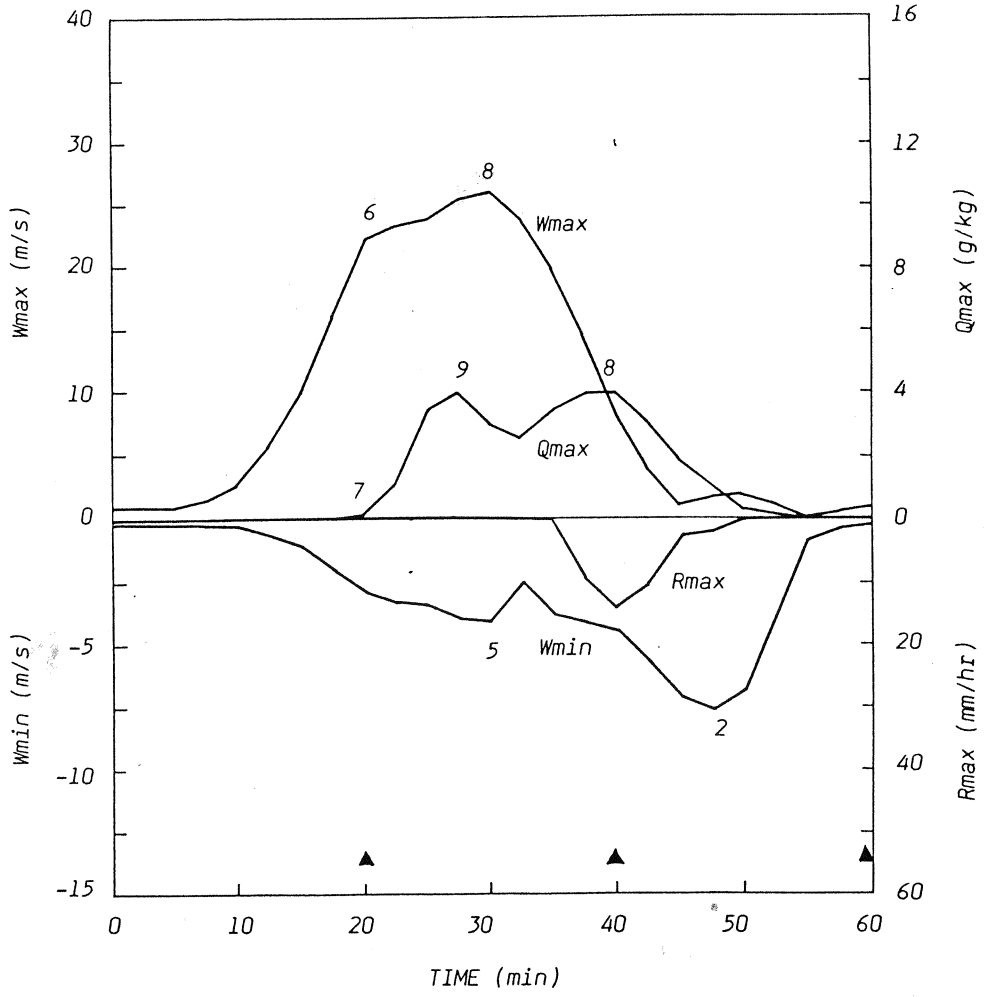

Fig. 9: C-case, time history.

4.2 Unidirectional shear case (S-case)

4.2.1 Growing stage (Figs. 10a-10j)

The growing stage in the sheared case is similar to the growing stage in the non-sheared case. However, the compensating downdraft develops mainly at the downwind side of the updraft and the perturbed temperature and pressure field patterns are displaced downwinds. Moreover, the low level air inflow relative to the storm movement is no more axially symmetrical - it takes place mainly from the downwind side. As a new feature, the vortex doublet is formed at intermediate levels.

4.2.2 Mature stage (Figs. 11a-11j)

Precipitating hydrometeors begin to fall out of the accumulation zone at the downwind side of the updraft. Due to the displacement relative to the updraft, the precipitation outfall and the associated updraft do not interact with the updraft significantly. The vortex doublet intensifies and the storm begins to split into two cells.

4.2.3 Dissipating stage (Figs. 12a-12j)

The low level inflow into the storm is cut off by the downdraft at the downwind side of the storm and the updraft - downdraft pair weakens. The vortex doublet also weakens and the precipitation outfall gradually ceases. At upper levels, some parts of the cloud top evaporate due to the air subsidence caused by the gravity wave.

4.2.4 General life history (Fig. 13)

The initial updraft growth is rapid, but its oscillations at the peak value are less pronounced. The maximum values of the updraft velocities decrease slowly with time. Updraft and downdraft are long-lived and their maxima are almost co-located in time.

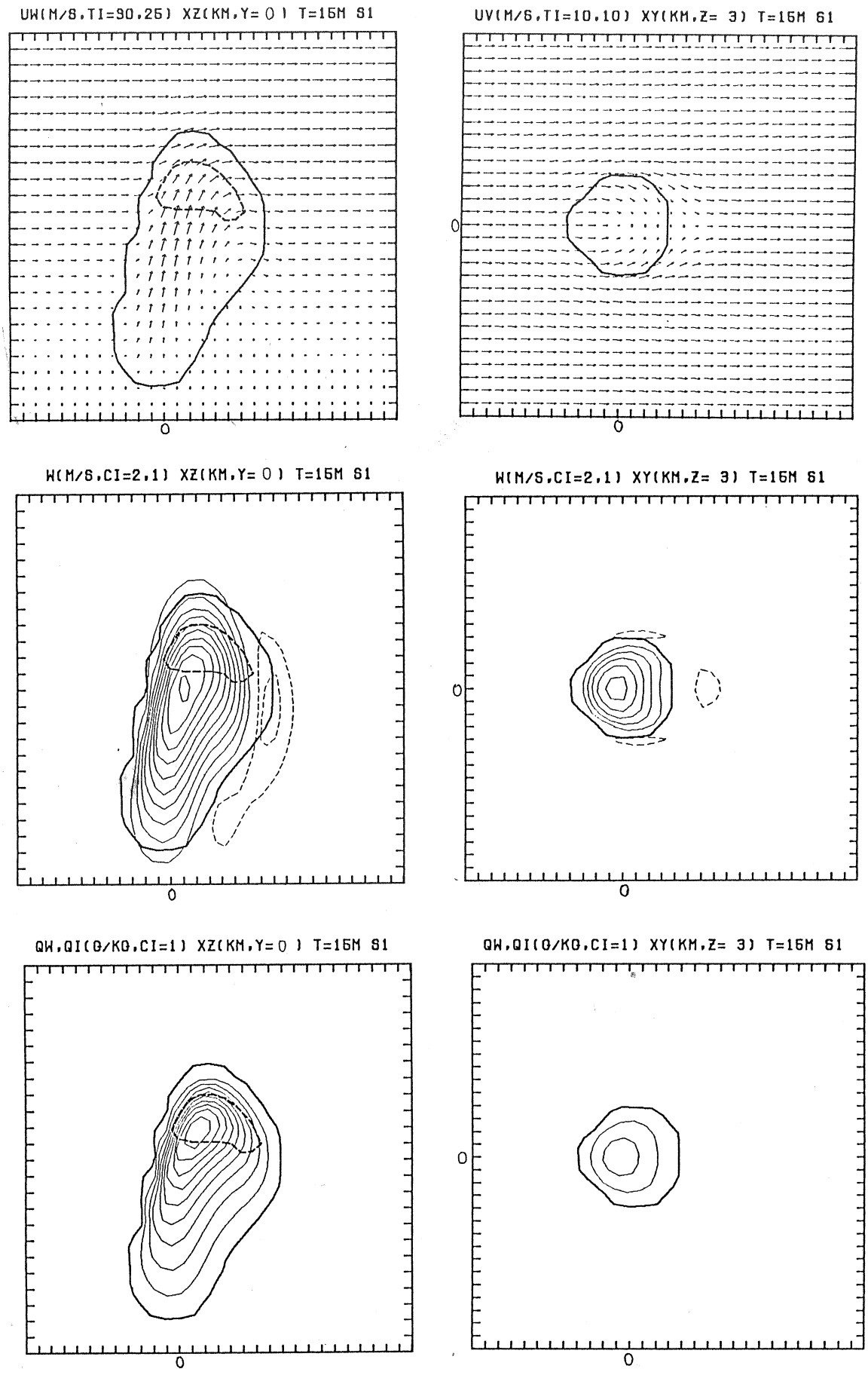

Figs. 10a - 10f: S-case, growing stage.

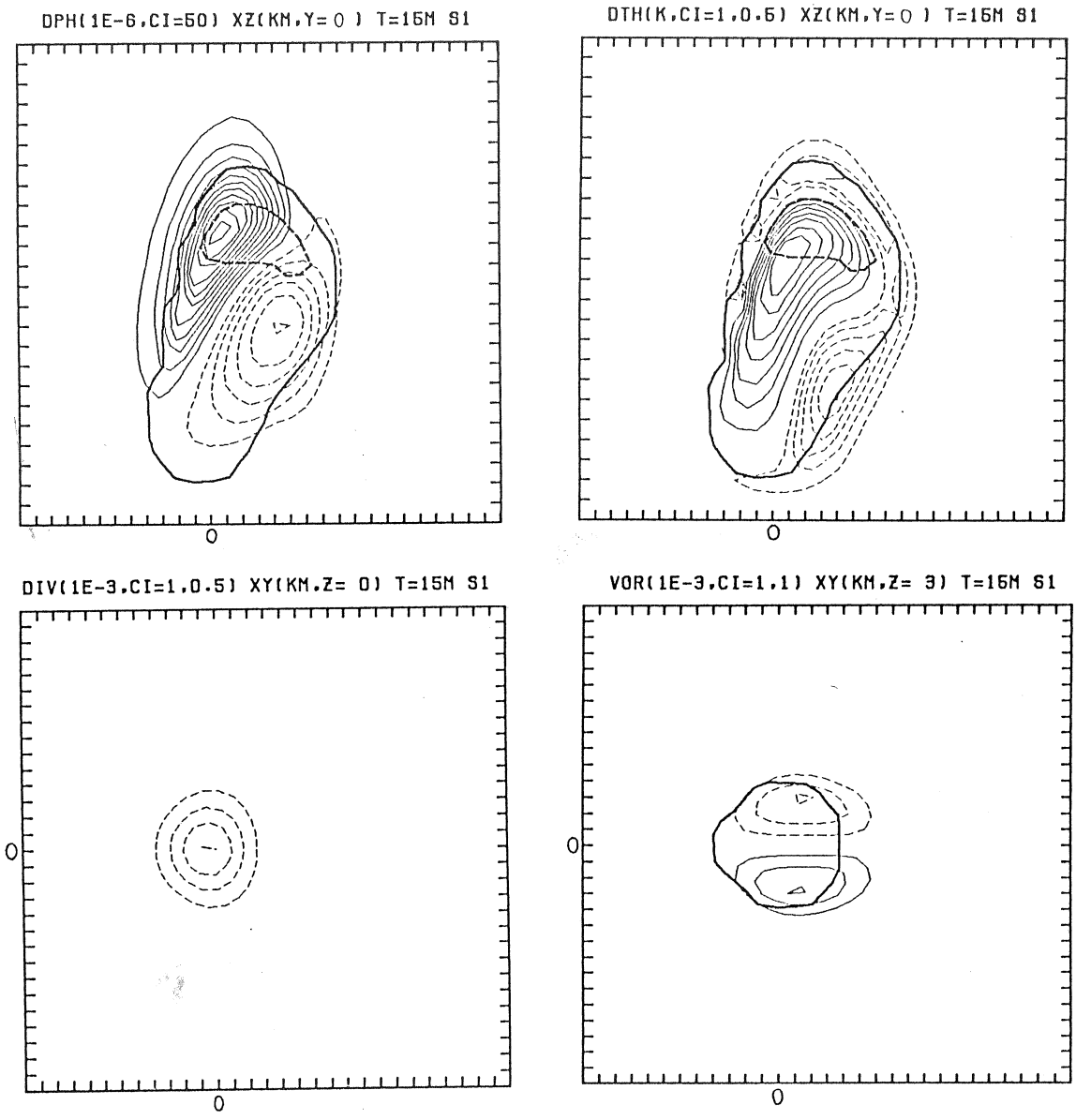

Figs. 10g - 10j: S-case, growing stage.

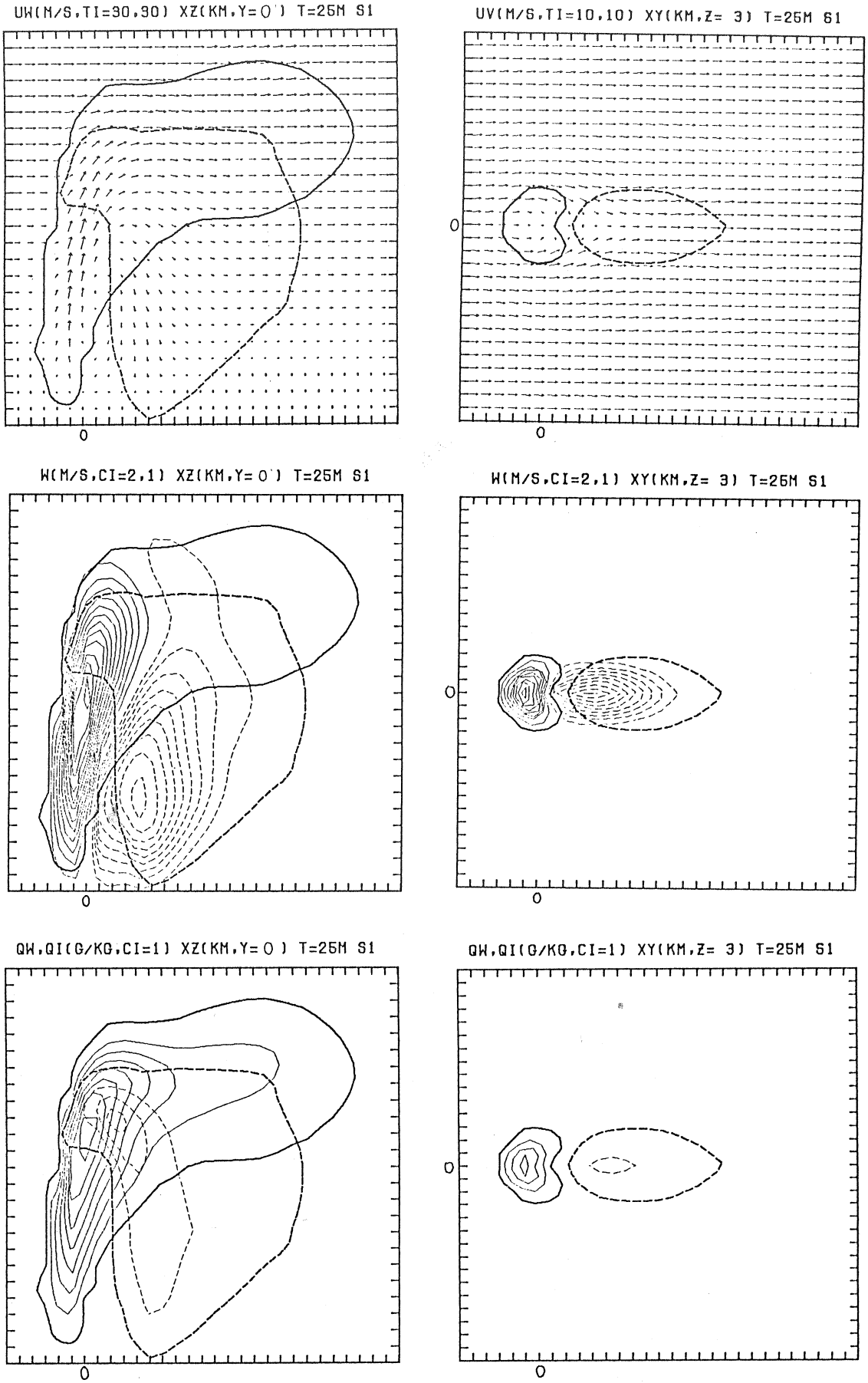

Figs. 11a - 11f: S-case, mature stage.

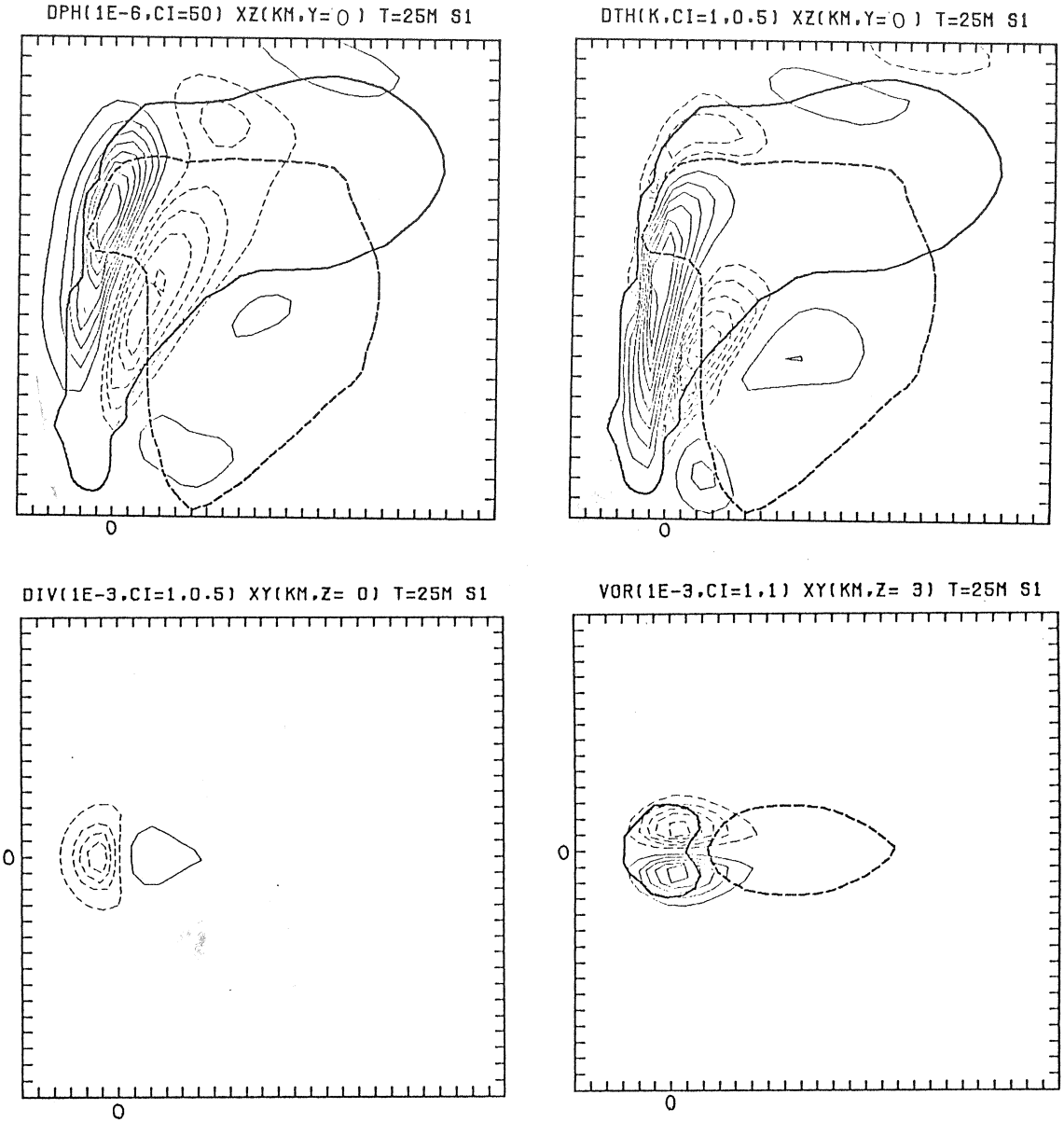

Figs. 11g - 11j: S-case, mature stage.

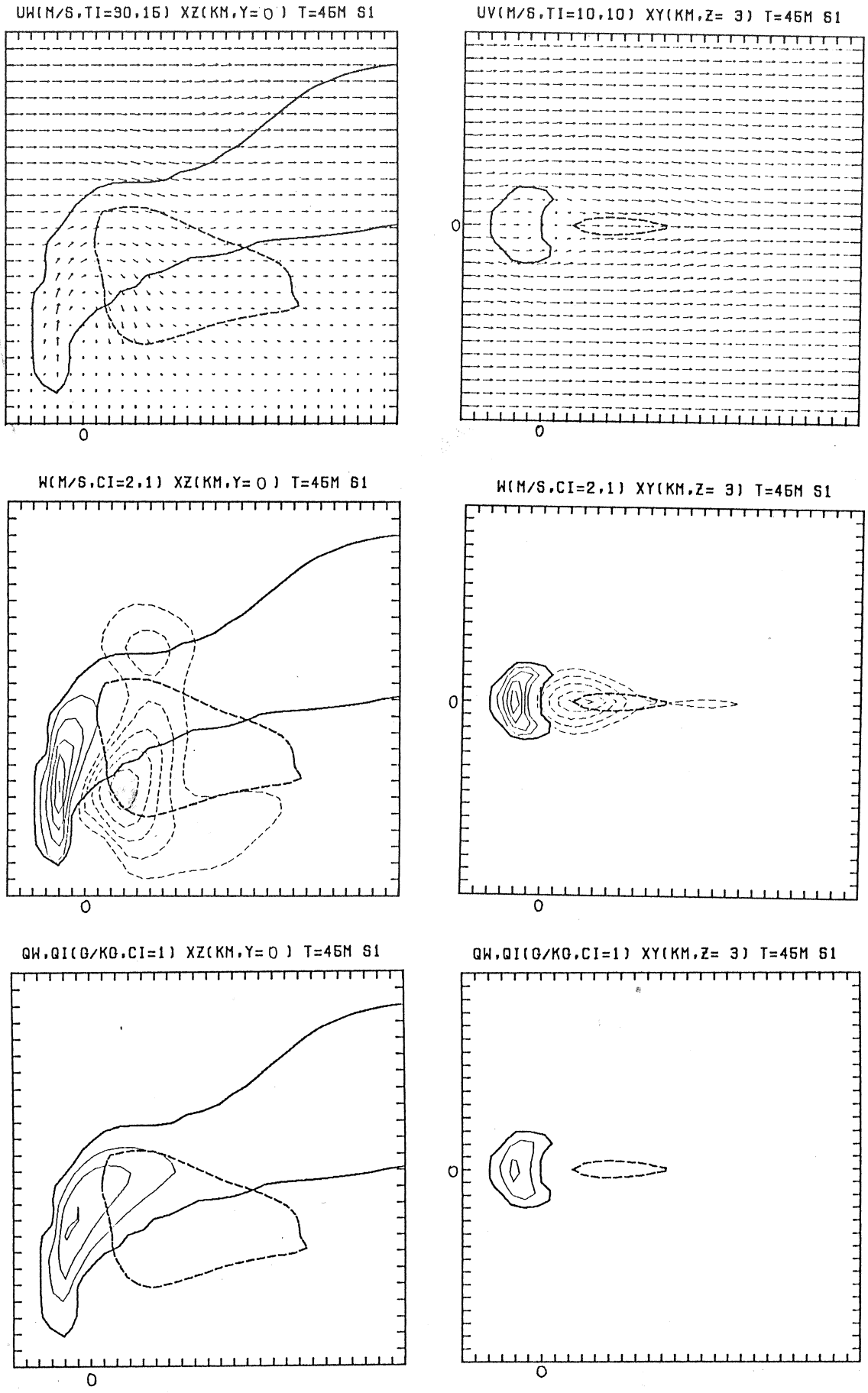

Figs. 12a - 12f: S-case, dissipating stage.

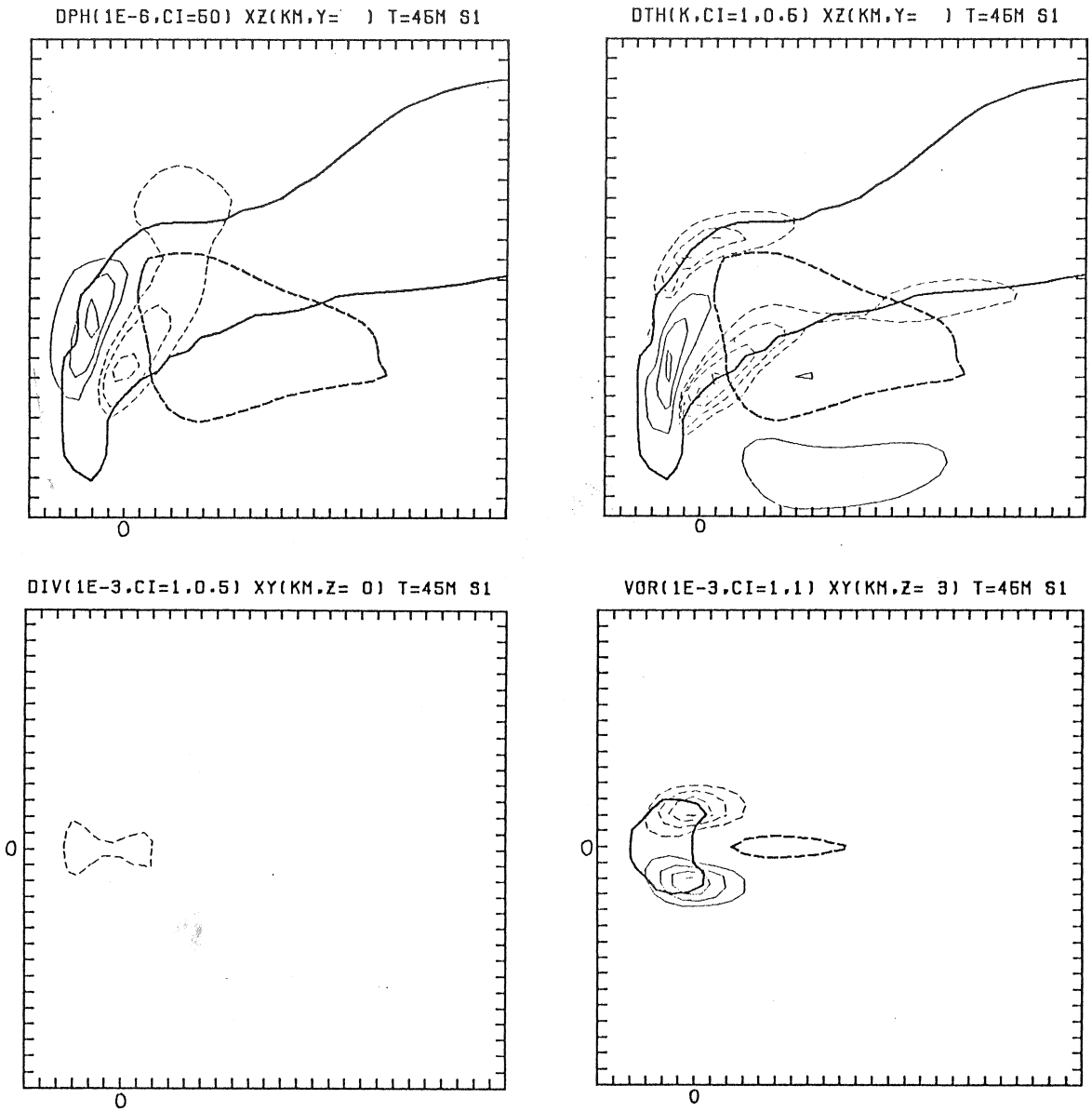

Figs. 12g - 12j: S-case, dissipating stage.

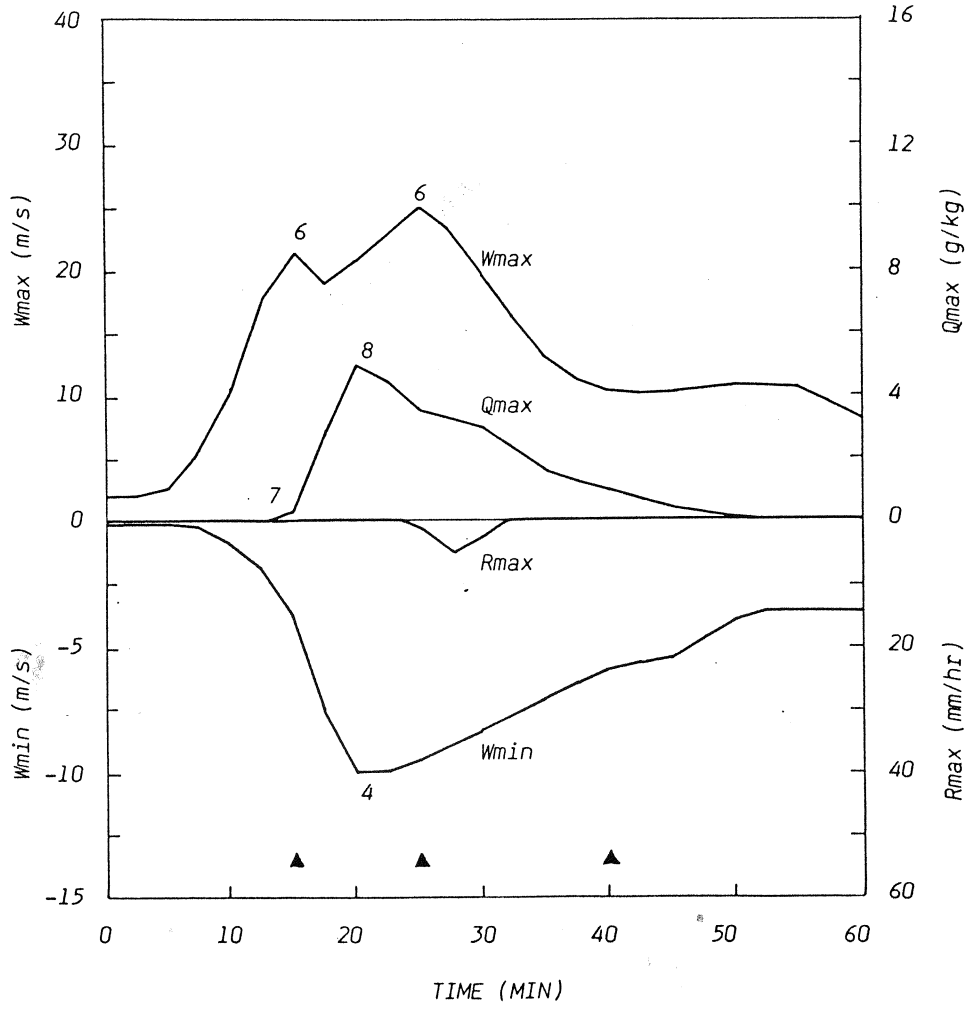

Fig. 13: S-case, time history.

4.3 Multidirectional shear case (V-case)

4.3.1 Growing stage (Figs. 14a-14j)

The growing stage in the veered case is basically the same as in the sheared case. The fields are no more plan-symmetrical: the low level inflow is located mainly at the right flank of the storm and the right flank vortex in the vortex doublet is developed stronger.

4.3.2 Mature stage (Figs. 15a-15j)

Precipitating hydrometeors, embeded in the downdraft, begin to fall out at the left flank of the storm, whereas the updraft maximum is found at the right storm flank. The vortex doublet intensifies and the storm begins to split into two cells.

4.3.3 Dissipating stage (Figs. 16a-16j)

The interaction between the downdraft spread-out at the low levels and the low level wind results in the low level convergence zone located at the right flank of the storm. From this convergence zone a new updraft emerges and a new cell growth occurs. The old cell dissipates slowly and the new cell intensifies.

4.3.4 General life history (Fig. 17)

The first part of the history for the veered case cloud is almost the same as for the sheared case cloud: rapid growth of the updraft, its small oscillation at its peak value and slow decrease thereafter, and the co-existence of the updraft and downdraft pair. In the second part, a regeneration of the updraft / downdraft pair occurs as the new convective cell is formed. The time history of the daughter cell closely resembles the history of its parent cell. However, the former cell does not reach such a vigorous mature stage as the latter one.

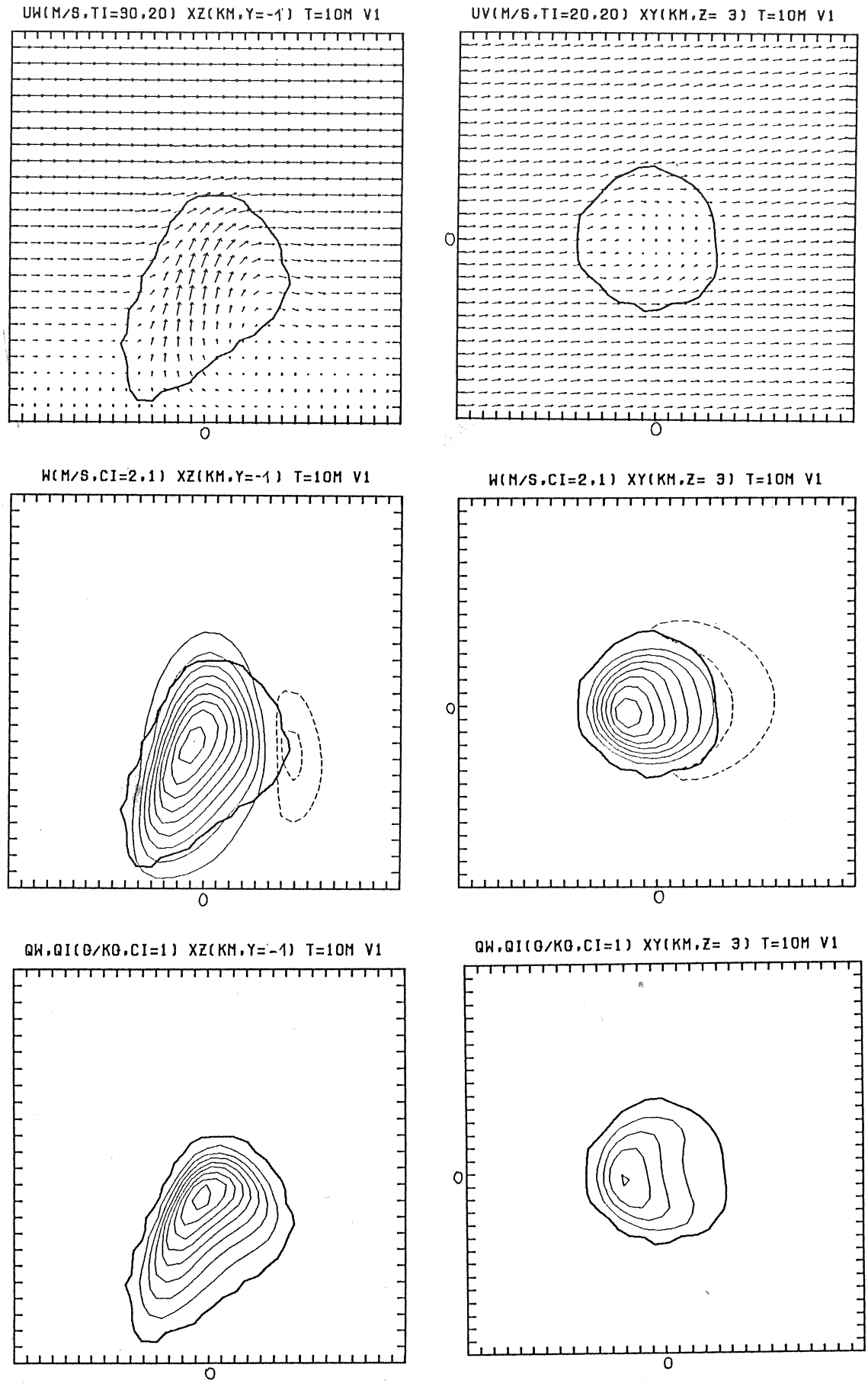

Figs. 14a - 14f: V-case, growing stage.

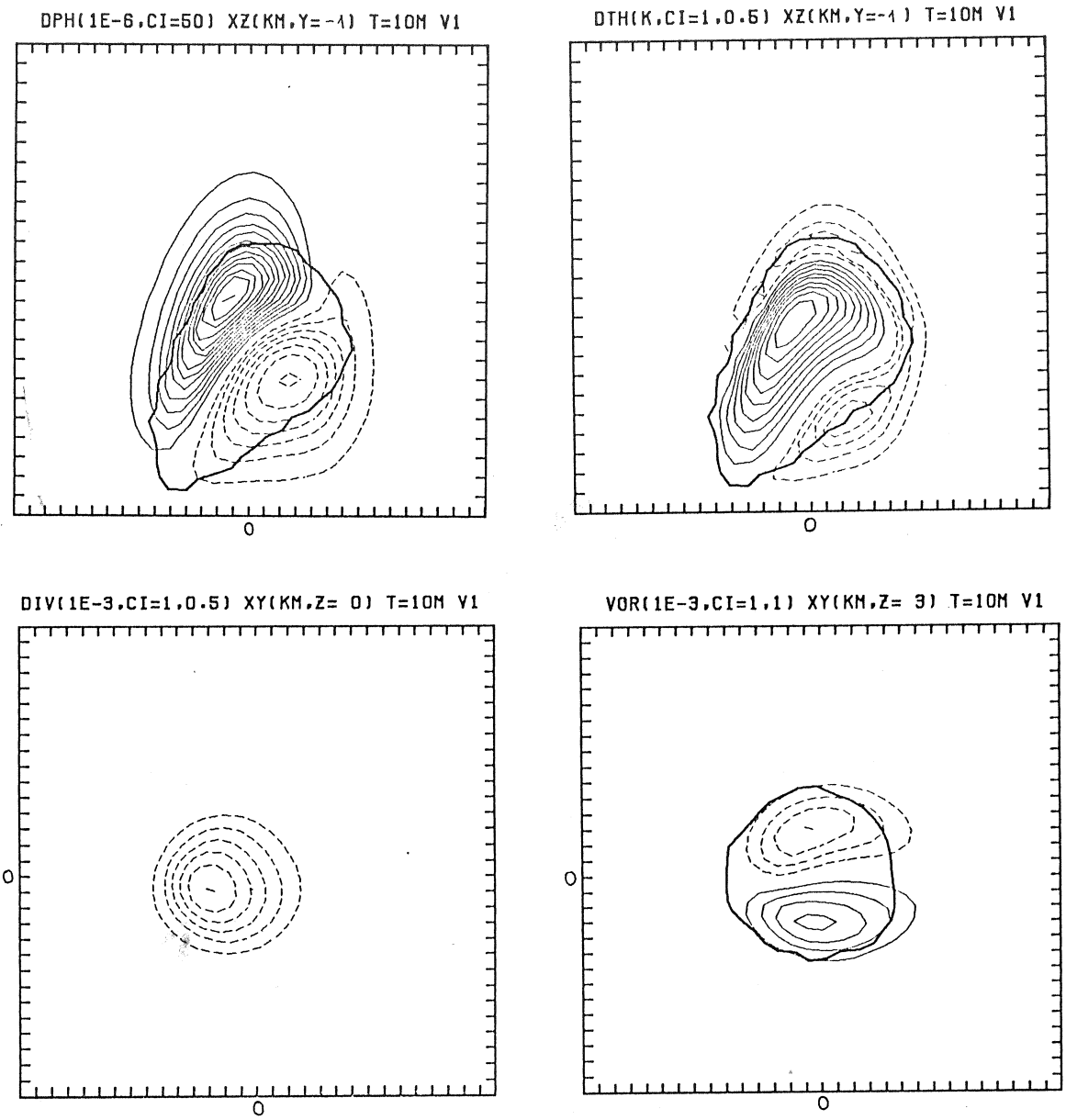

Figs. 14g - 14j: V-case, growing stage.

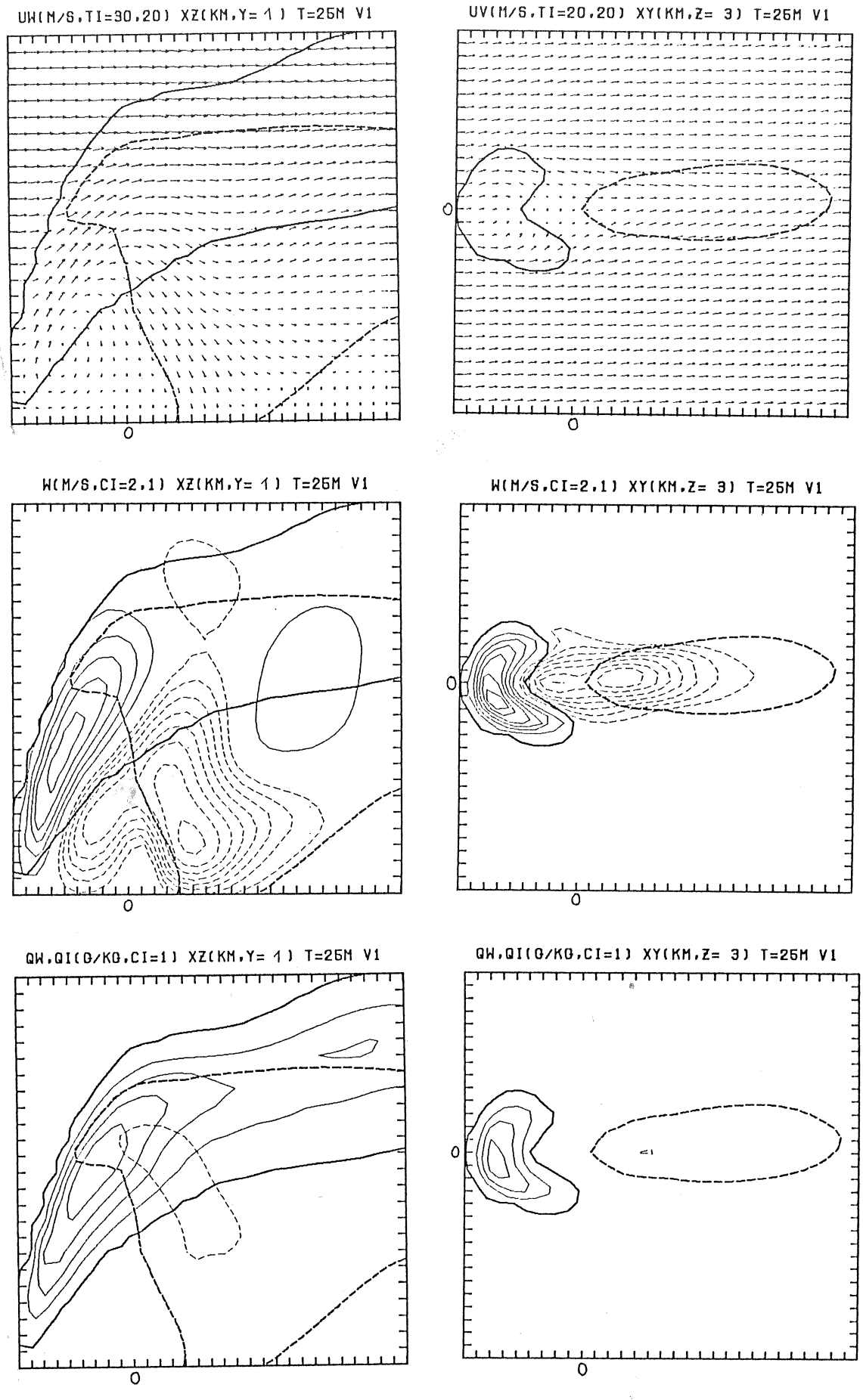

Figs. 15a - 15f: V-case, mature stage.

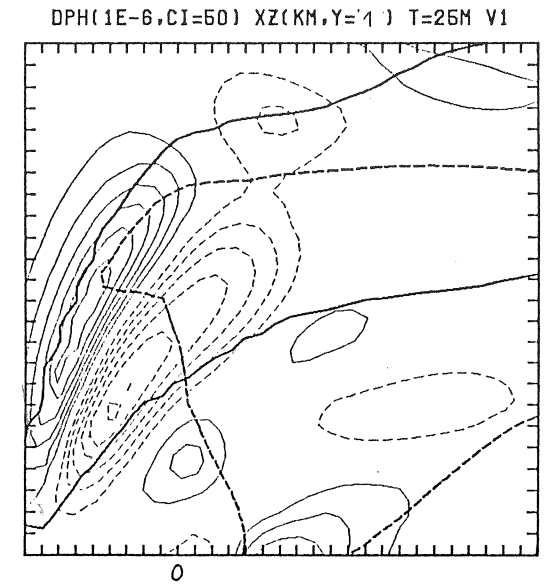

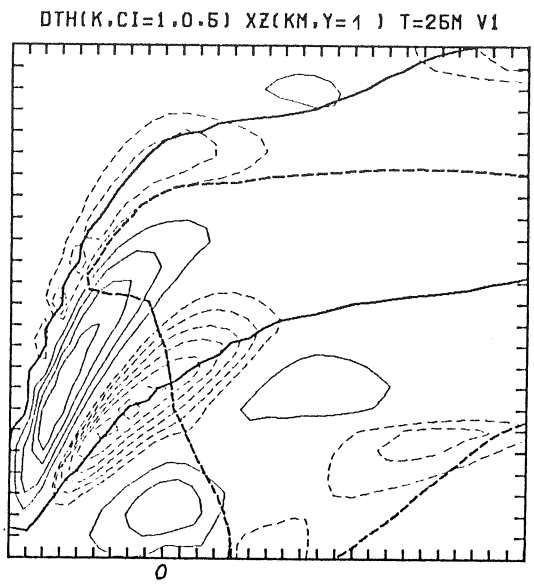

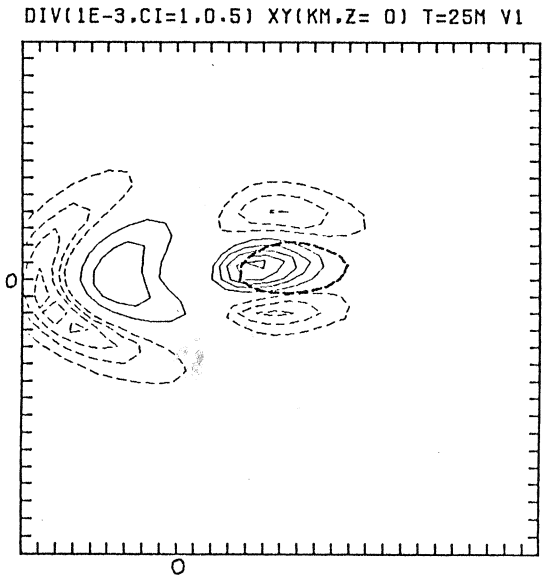

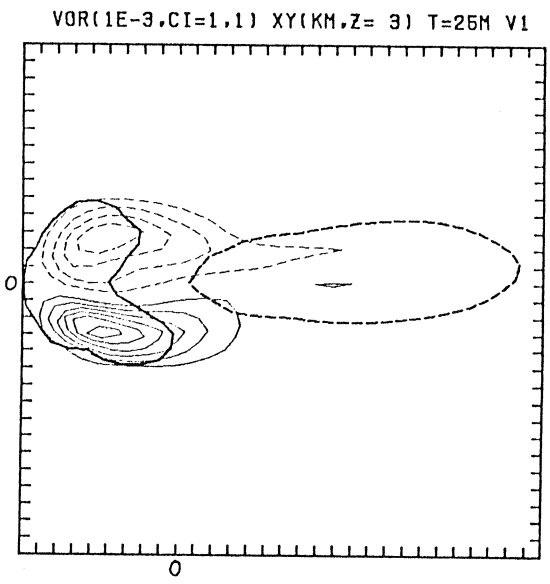

Figs. 15g - 15j: V-case, mature stage.

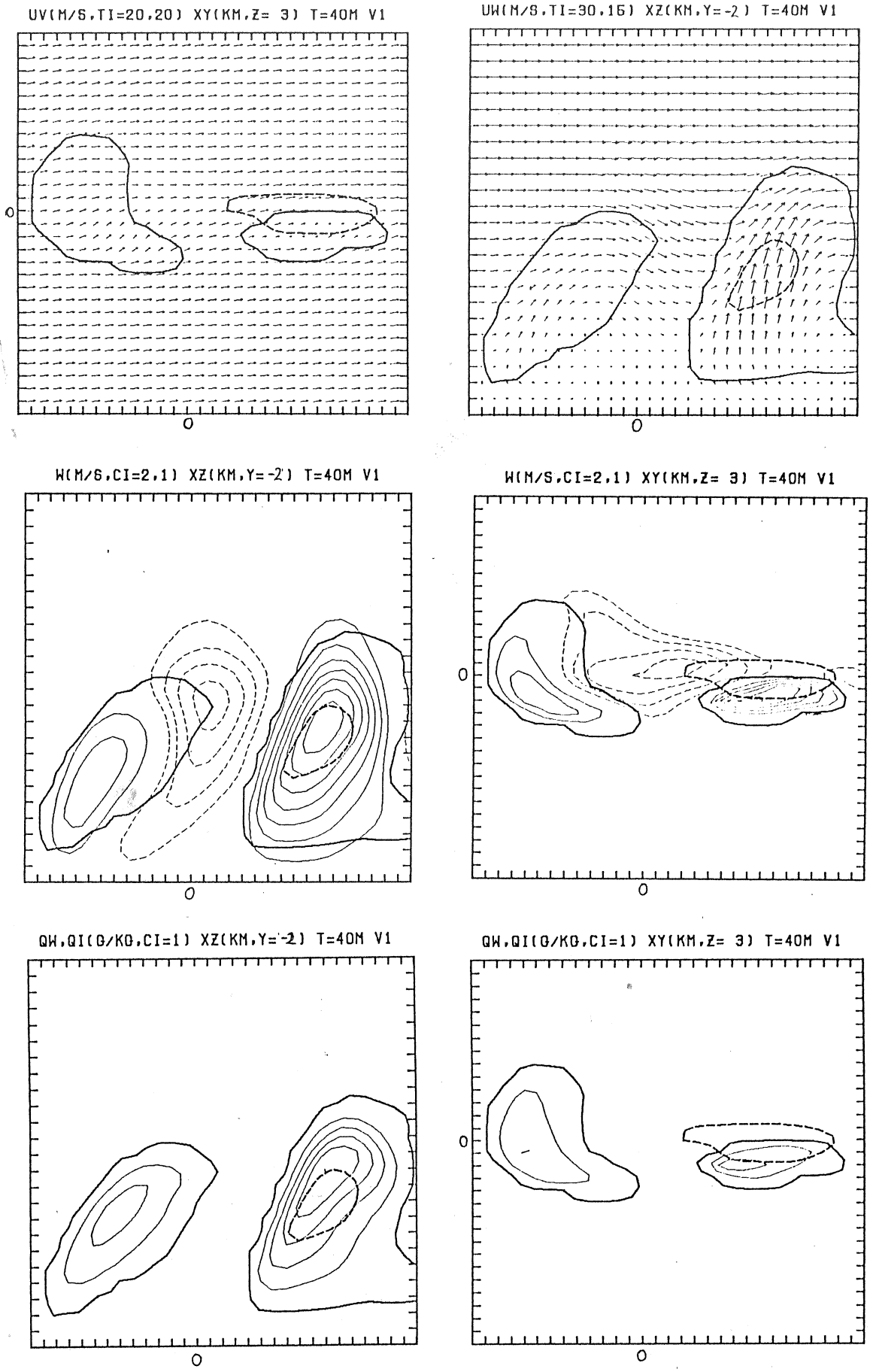

Figs. 16a - 16f: V-case, new growth stage.

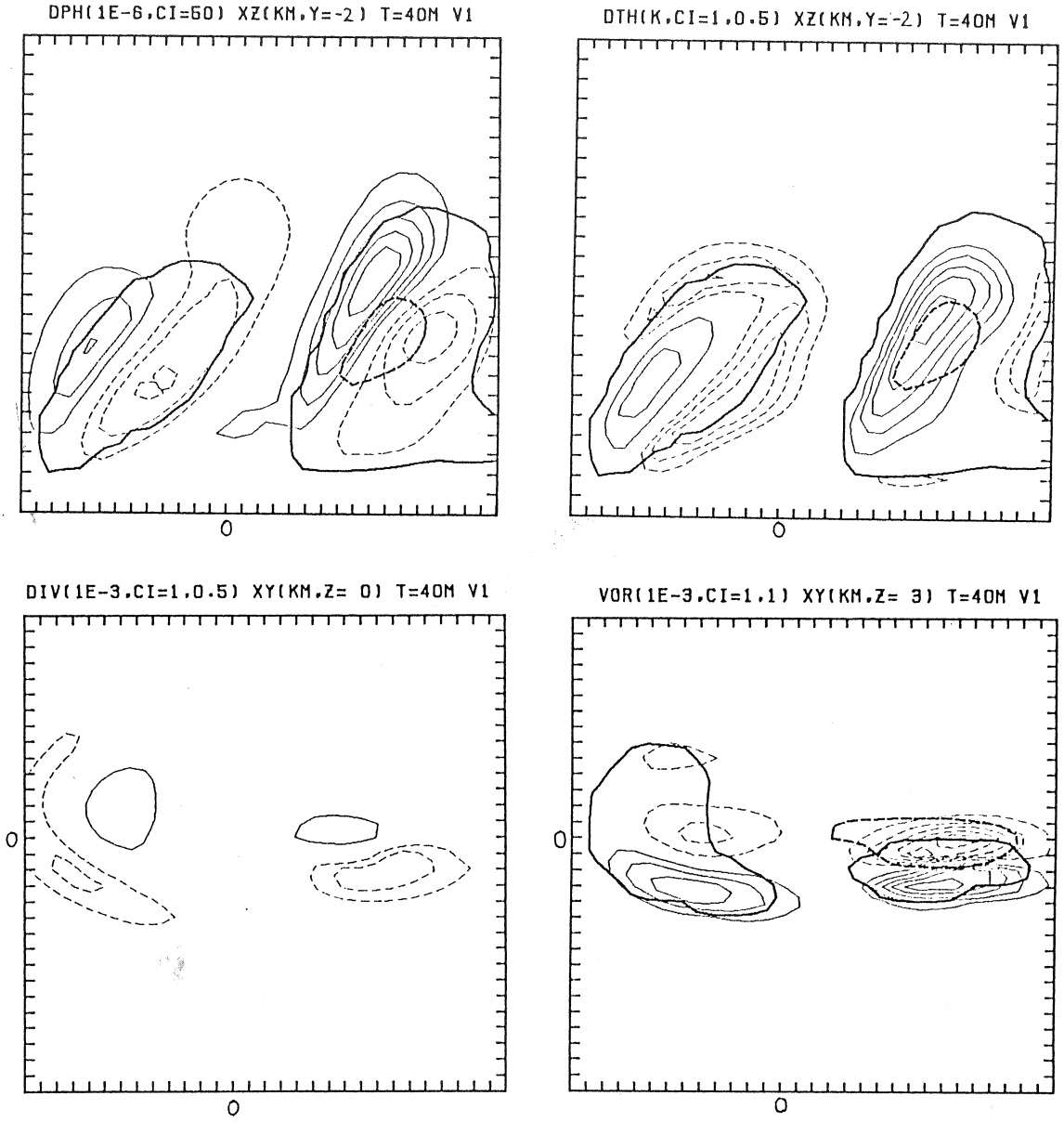

Figs. 16g - 16j: V-case, new growth stage.

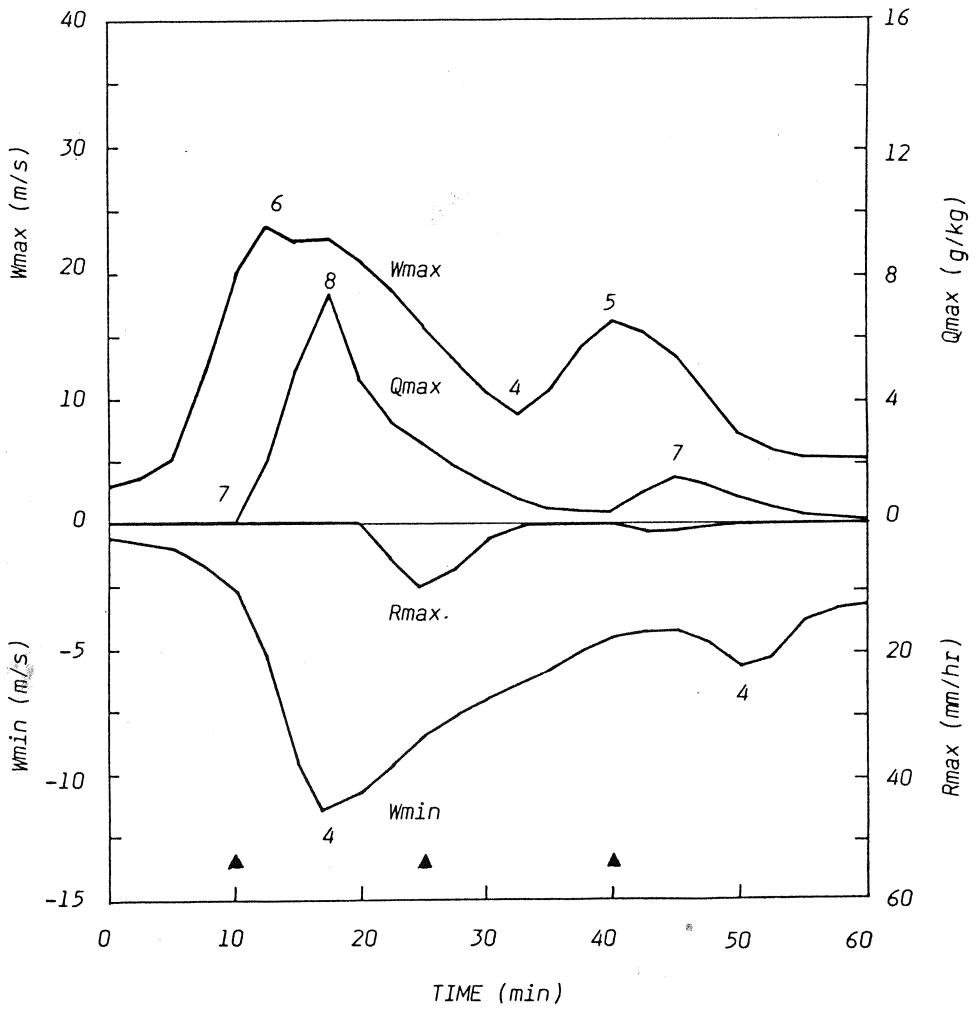

Fig. 17: V-case, time history.

5. SUMMARY AND CONCLUSIONS

The development of an isolated convective storm in an ambient wind field is studied using a three-dimensional numerical model.

Three experiments are run with different vertical profiles of ambient wind: no shear, positive speed shear but no directional shear, and positive speed shear with low level veering. In all cases, the same vertical profiles of temperature and humidity are used. Convection is triggered by the initial temperature and momentum perturbation in a form of a shallow radial symmetric warm updraft. The cases are investigated in regard to airflow, pressure, temperature, and precipitation patterns. The following is found.

1. The growing stage is weaker with shear than without, and to trigger the convection of nearly the same intensity of the mature stage, stronger initial perturbations are needed for cases with shear than without it. The mature stage in the sheared environment is more persistent. Without shear, the main downdraft develops directly beneath the updraft, whereas with shear the main downdraft develops downwinds of the updraft.

2. An internal gravity wave is triggered at upper levels when the cloud top approaches the tropopause.

3. Sheared storms exhibit a nearly erect updraft, a vortex doublet aloft, middle level barrier flow around the updraft, and gradual splitting into two cells.

4. During the growing stage, the perturbed pressure field exhibits a meso-low under the cloud, and a meso-high near its top. With shear, the meso-low is displaced downwinds of the meso-high. During the mature stage, highs are found beneath the downdraft and at the updraft summit, and low at intermediate levels.

5. Thermal buoyancy and the perturbed vertical pressure gradient force oppose each other.

6. With perturbations used, secondary convection develops in the neighbourhood of the downdraft only in the veered environment. New cell growth occurs at the right flank.

ACKNOWLEDGMENTS

Most of this work was carried out while I was working at the Nagoya University Water Research Institute. I would like to thank Prof. Takao Takeda for his general guidance and support during the development of the numerical model described in this report. I also greatly appreciate the programming help of Shinichi Tanahashi. I wish to thank to everybody at the Department for the Atmospheric Environment, Water Research Institute, for their help and interest in my work.

REFERENCES

Clark, T. L., 1973:
Numerical modeling of the dynamics and microphysics of warm cumulus convection. J. Atmos. Sci., 30, 857-878.

----, 1979:
Numerical simulations with a three - dimensional cloud model: Lateral boundary condition experiments and multicellular severe storm simulations. J. Atmos. Sci., 36, 2191-2215.

Klemp, J. B., R. B. Wilhelmson and P. S. Ray, 1981:
Observed and numerically simulated structure of a mature supercell thunderstorm. J. Atmos. Sci., 38, 1558-1580.

----, and R. B. Wilhelmson, 1978:
The simulation of three - dimensional convective storm dynamics. J. Atmos. Sci., 35, 1070-1096.

Ogura, Y. and N. W. Phillips, 1962:
Scale analysis of deep and shallow convection in the atmosphere. J. Atmos. Sci., 19, 173-179.

Schlesinger, R. E., 1975:
A three-dimensional numerical model of an isolated deep convective cloud: Preliminary results. J. Atmos. Sci., 32, 934-957.

----, 1978:
A three-dimensional numerical model of an isolated thundestorm: Part I. Comparative experiments for variable ambient wind shear. J. Atmos. Sci., 35, 690-713.

----, 1980:
A three-dimensional numerical model of an isolated thunderstorm: Part II. Dynamics of updraft splitting and mesovortex couplet evolution. J. Atmos. Sci., 37, 395-420.

Steiner, J. T., 1973:
A three-dimensional model of cumulus cloud development. J. Atmos. Sci., 30, 414-435.

Takeda, T., 1971:
Numerical simulation of a precipitating convective cloud: The formation of a "long-lasting" cloud. J. Atmos. Sci., 28, 350-376.

Wilhelmson, R. and Y. Ogura, 1972:
The pressure perturbation and the numerical modeling of a cloud. J. Atmos. Sci., 29, 1295-1307.

----, 1974:
The life cycle of a thunderstorm in three dimensions. J. Atmos. Sci., 31, 1629-1651.

----, and J. B. Klemp, 1981:
A three-dimensional numerical simulation of splitting severe storm on 3 April 1964. J. Atmos. Sci., 38, 1581-1600.

Wisner, C., H. D. Orville and C. Mayers, 1972:
A numerical model of a hail-bearing cloud. J. Atmos. Sci., 29, 1160-1181.